*Journal of the Korean Nuclear Society*
*Volume 34, Number 1, pp.30~41, February, 2002*

# Beam Characteristics of Polychromatic Diffracted Neutrons Used for Prompt Gamma Activation Analysis

**S. H. Byun, G. M. Sun, and H. D. Choi**
Seoul National University
San 56-1 Shillim-dong, Kwanak-gu, Seoul, 151-742, Korea
E-mail : vandegra@gong.snu.ac.kr

(Received September 7, 2001)

## Abstract

The neutron beam is fully characterized for the prompt gamma activation analysis facility at Hanaro in the Korea Atomic Energy Research Institute(KAERI). The facility uses thermal neutrons which are diffracted vertically from a horizontal beam port by a set of pyrolytic graphite(PG) crystals positioned at the Bragg angle of 45°. Neutron spectra, neutron flux and Cd-ratio are determined for the three extraction modes of diffracted beam by means of the theoretical and experimental efforts. To obtain theoretical result, the reflectivity of pyrolytic graphite is calculated in the diffraction model for mosaic crystal and the angular divergence after diffraction by mosaic crystal is estimated from Monte Carlo simulation. The time-of-flight spectrometer and gold activation wire are used for measuring the neutron spectra. Both the calculated and measured spectra have proven that the unique feature of polychromatic beam obtained by PG crystals are useful for PGAA. The thermal neutron flux of $7.9 \times 10^7$ n/cm$^2$s and the Cd-ratio of 266 for gold have been achieved at the sample position while the reactor operates at 24 MW. The uniformity of beam flux is 12% in the central $1 \times 1$ cm$^2$ area. Finally, the beam is briefly characterized by the effective velocity and temperature which are determined by measuring the prompt γ-ray spectra for thin and thick boron samples.

**Key Words** : Prompt Gamma Activation Analysis, Bragg diffraction, pyrolytic graphite

## 1. Introduction

The Prompt Gamma Activation Analysis(PGAA) is a radio-analytical method which can determine concentrations of component nuclides in a sample by detecting the prompt γ-rays emitted after the neutrons are absorbed. The performance of a PGAA facility depends on obtaining a high flux thermal or cold neutron beam with backgrounds of fast neutron and γ-ray removed to a sufficient level. The pioneering facilities mostly adopt direct neutron beam[1] from the beam port or filtered beam[2], while the recent trend is developing facility by using the mirror guided beam[3-7].

The PGAA facility in KAERI has been operational since May 2001. Developing this facility was initiated and funded by the request of $^{10}$B analysis along with developing the Boron

Neutron Capture Therapy(BNCT) facility in Hanaro, KAERI. The major task was performed by Seoul National University(SNU), and hence the facility is referred to as the SNU-KAERI PGAA facility in this paper. Due to the initial difficulty of assigning a beam port for the facility, the method of Bragg diffraction by using pyrolytic graphite(PG) crystals is adopted for extracting thermal neutrons from a direct beam port[8,9] and therefore enables sharing of neutron beam port with other device. The Bragg angle of 45° is used to reduce scattered fast neutrons and ease beam line construction although higher flux can be expected for smaller angles. The unique feature of the facility is that polychromatic diffracted neutrons are utilized without filtration[10-12] while the monochromatic diffracted beam is being used for the existing facilities in refs. 8 and 9.

The SNU-KAERI PGAA facility has been installed on a platform located at the exit of 4 m long ST1 tangential beam port. The angular divergence of the white beam is defined by a set of Soller collimators positioned near the exit of the beam port inside the reactor wall. No collimation by full open position is used to obtain the maximum beam flux while the collimation by 20′ or 30′ condition is available for choosing a reduced beam flux at the sample. The cross section of the ST1 beam port is $70^{w} \times 120^{h}$ mm$^2$, among which the central part of $70^{w} \times 60^{h}$ mm$^2$ is used for the polarized neutron spectrometer, while the peripheral areas at the top and bottom edges are assigned to the PGAA facility. PG crystals mounted on a goniometer are covering the areas of edge regions of the ST1 beam cross section. One layer of crystal is 2 mm thick, 75 mm wide and 50 mm long. Two layers of crystals are mounted on each edge. To obtain maximum flux at the sample position, the mosaic spread of crystal is optimized to 0.8°[11] and the focusing technique for diffracted beam is applied[13-15] by placing and tuning three pieces of crystals in concave form. The sample position is about 1.5 m vertically upwards from ST1 port center axis. The progress of developing the SNU-KAERI PGAA facility has been reported in the previous meetings of the Korean Nuclear Society[16-18]. The present paper discusses in detail the characteristics of diffracted neutron beam for the SNU-KAERI PGAA facility. The full description of the overall facility including the γ-ray spectrometer is given in a separate paper[19].

## 2. Theoretical Considerations

### 2.1. Diffracted Neutron Spectrum and Flux

The mosaic crystals have been used for obtaining monochromatic neutron beam since the advent of the neutron scattering technique. The well-known Bragg diffraction takes place from the mosaic crystal whenever the wavelength of the incident neutron satisfies the Bragg rule,

$$2d \sin \theta_B = n\lambda_n \tag{1}$$

where $d$ is the interplanar spacing of crystallographic planes, $\theta_B$ is the Bragg angle, $\lambda_n$ is the wavelength of neutron and $n$ is the diffraction order. The reflectivity of a mosaic crystal is described theoretically by the Darwin equations[20]. The solutions of Darwin equations for nonabsorbing crystals have been given by Bacon and Lowde[21] while Sears has studied the general solution recently[22]. The angular distribution of the mosaic blocks' orientation is usually assumed to be a Gaussian

$$W(\Delta) = \frac{1}{\eta\sqrt{2\pi}} e^{-\Delta^2/2\eta^2} \tag{2}$$

where $\Delta$ is the angle between the normal of a mosaic block and that of the crystal surface, and $\eta$

is the standard deviation of the distribution, which is related to the mosaic spread $\beta$, the FWHM of $W(\Delta)$, by

$$\beta = 2\eta\sqrt{2\ln 2}\,. \tag{3}$$

Pyrolytic graphite has highly preferred orientation only for (002) plane while all the other planes are aligned at random. The interplanar spacing between (002) planes is 3.354 Å for PG crystal. Pyrolytic graphite belongs to the class of nonabsorbing crystals with symmetric reflection and the solution of the Darwin equations gives the reflectivity as[21,22]

$$R(\Delta) = Q\frac{t_0}{\sin\theta_B}W(\Delta)\left[1+Q\frac{t_0}{\sin\theta_B}W(\Delta)\right]^{-1} \tag{4}$$

where $t_0$ is the crystal thickness and $Q$, the crystallographic quantity, is given for PG crystal[13],

$$Q = (\lambda_n{}^3/\sin 2\theta_B)5.65\times 10^{-3} \quad [\mathrm{cm}^{-1}] \tag{5}$$

when the neutron wavelength is expressed in [Å]. The reflectivity at $\Delta$=0 is given by

$$R(0) = \frac{1}{\eta\sqrt{2\pi}}\frac{Qt_0}{\sin\theta_B}\left[1+\frac{1}{\eta\sqrt{2\pi}}\frac{Qt_0}{\sin\theta_B}\right]^{-1} \tag{6}$$

and it gives the peak reflectivity. The integrated reflectivity $R^\theta$ is the integration of R($\Delta$) over all $\Delta$ range and an exact value is obtained only by numerical integration. An approximate form of $R^\theta$ is given by

$$R^\theta = 0.61(\beta Qt_0/\sin\theta_B)^{1/2} \tag{7}$$

showing that $R^\theta$ is proportional to the square root of the mosaic spread and the thickness. The dimension of the integrated reflectivity can be converted to wavelength by using the differential form of eq. (1) and converted even further to energy. Hence the integrated reflectivity in energy scale, $R^E$, is

$$R^E = 2R^\theta E_n \cot\theta_B\,. \tag{8}$$

By considering the divergence effect after diffraction, the diffracted neutron flux from order $n$ becomes

$$\phi_D(n) = \phi_{in}(E)R^E f_1 f_2\,, \tag{9}$$

where $\phi_{in}(E)$ is the differential flux of the incident beam, $f_1$ and $f_2$ are the divergence factors representing the decrease of the diffracted neutron flux due to the angular divergence effect after diffraction. Here, the subscript 1 and 2 correspond to the divergence in the diffraction plane and the plane perpendicular to the diffraction plane, respectively. Divergence factors are determined from the calculated beam profile which is obtained by a simple Monte Carlo program[17].

For the Bragg condition met, most of scattered neutron originates from Bragg diffraction while incoherent scattering also takes place. For graphite, only the coherent Bragg scattering contributes to the elastic scattering since the incoherent scattering cross section is zero[23].

The calculated reflectivity of 0.8° PG crystal with 4 mm thickness is shown in Fig. 1 for several diffraction orders. The peak reflectivity approaches to 1.0 for the 1st order and gradually decreases for higher orders. In Fig. 2, the theoretical prediction of polychromatic spectrum is shown upto 1 eV. The incident white neutron spectrum is assumed by the Maxwellian of 308 K and of 1/$E$-shape above 0.3 eV. The integrated incident spectrum is normalized to the measured thermal flux and Cd-ratio at the end of ST1 port. The diffracted flux for $n$=3 is the highest due to the high differential incident flux even though its reflectivity is lower than that for $n$=1 or 2. The total diffracted flux is $4.1\times 10^7$ n/cm$^2$s, which

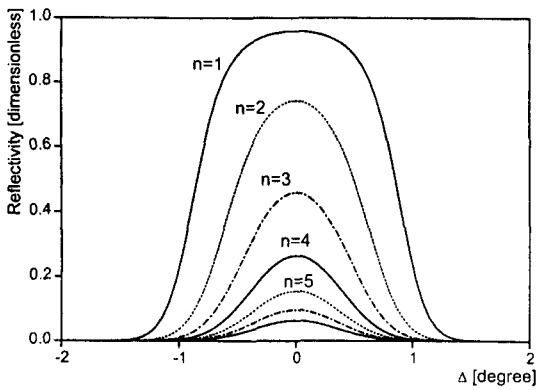


**Fig. 1. Reflectivity of a 0.8° Graphite Crystal with 4 mm Thickness Set at the Bragg Angle of 45°.**

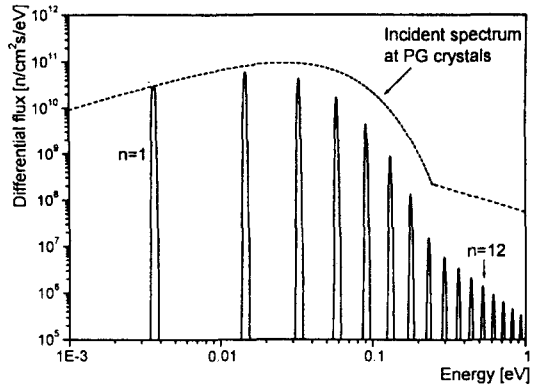


**Fig. 2. Diffracted Neutron Spectrum Calculated for a 0.8° Graphite Crystal with 4 mm Thickness Set at the Bragg Angle of 45°.**

was obtained by summing all orders. The summation was saturated about $n$=6. The sum of orders 2, 3 and 4 is comprising 84% of the total diffracted beam. The energy width of the diffracted beam originates from the mosaic spread and incident beam spread, and is proportional to the beam energy. The energy and width for the 3rd order is 32.8±1.5 meV. Hence diffracted beam of each order can be regarded mono-energetic.

A detailed theoretical model includes the consideration of the thermal vibration effects in the scattering process. The lattice vibration reduces the diffracted neutrons and causes the inelastic thermal diffuse scattering(TDS). The reduction of diffracted neutron is described by the Debye-Waller factor and the small increase of neutron by TDS is represented by a correction factor. Whereas the Debye-Waller factors are accurately known for cubic crystals, this is not the case for graphite[24]. Accordingly, TDS correction is also difficult for graphite crystal. Hence the two effects are approximated to cancel out in this study. Since the vibration effects are more severe for high diffraction orders, the theoretical diffracted spectrum in Fig. 2 is less reliable in epithermal region.

## 2.2. Cd-ratio and Effective Quantity for Diffracted Beam

To evaluate the portion of epithermal neutrons in total neutron flux at the sample position, the Cd-ratio of $^{197}$Au is calculated theoretically. Since the conventional Cd cutoff energy depends on the details of the neutron spectrum and the thickness of the used Cd, a general expression for Cd-ratio is considered instead of integration with a proper Cd cutoff energy. The Cd-ratio of a nuclide for narrow neutron beam is defined as the absorption rate of bare nuclide to that of Cd covered and given by

$$R_{Cd} = \frac{\int_0^\infty \phi(E)\sigma_a(E)dE}{\int_0^\infty e^{-\Sigma_a(E)t}\phi(E)\sigma_a(E)dE}, \qquad (10)$$

where $\phi(E)$ is the differential beam flux incident on the target, $\sigma_a(E)$ is the absorption cross section of the nuclide, $\Sigma_a(E)$ is the macroscopic absorption cross section of Cd and $t$ is the thickness of the Cd sheet. For the beam spectrum in this study, most of the bare absorption rate originates from the polychromatic diffracted beam in the thermal energy region and therefore the numerator is simplified to

$$\int_0^\infty \phi(E)\sigma_a(E)dE \cong \sum_{n=1}^{6} \phi_D(n)\sigma_a(E_n), \quad (11)$$

where the summation is accurate enough by taking upto the 6th order. Similarly, the denominator in eq. (10) is represented as

$$\int_0^\infty e^{-\Sigma_a(E)t}\phi(E)\sigma_a(E)dE = \sum_{n=1}^{\infty} e^{-\Sigma_a(E_n)t}\phi_D(n)\sigma_a(E_n). \quad (12)$$

The summation is performed for 0.5 mm thick Cd upto 30 eV to fully cover the resonance region of $^{197}$Au. The cross sectional data is obtained from ENDF database[25]. Due to the discrete nature of the diffracted beam, proper calculation of the exponential factor, especially in the epithermal region is necessary for accurate calculation of Cd-ratio. The neutron energies corresponding to 10% and 90% transmission from 0.5 mm Cd are 0.3 eV and 0.7 eV, respectively. The diffraction orders of $n$=9 to $n$=14 belong to this energy region. The calculated Cd-ratios change slightly with the extraction condition of diffracted beam and are in the range of 260 ~ 300. The result has been refined from the previous value[11] by considering the contribution of high order diffracted epithermal flux.

The effective absorption cross section for an absorber nuclide is defined as the cross section averaged for beam spectrum and can be simplified for the diffracted beam to

$$\langle\sigma_a\rangle = \frac{1}{\phi}\int_0^\infty \sigma_a(E)\phi(E)dE \cong \sum_{n=1}^{6} w_n\sigma_a(E_n), \quad (13)$$

where $w_n$ is the relative fraction of $n$-th order component flux in the total diffracted beam flux. For an $1/v$-absorber, the effective velocity of the neutrons is given by

$$\langle v\rangle = v_0\frac{\sigma_{a0}}{\langle\sigma_a\rangle}, \quad (14)$$

where $v_0$ is 2200 m/s and $\sigma_{a0}$ is the absorption cross section at $v_0$. The effective wavelength and effective temperature of the beam are given correspondingly.

**Table 1. Detailed Conditions for the Three Extraction Modes of Diffracted Beam.**

| Extraction mode | White beam collimation | Number of crystal layer | Crystal shape |
|---|---|---|---|
| 1 | Full open | 1 | Flat |
| 2 | Full open | 2 | Flat |
| 3 | Full open | 2 | Focusing |

## 3. Experimental Characterization

The experimental characterization of the diffracted beam has been performed for the three kinds of extraction modes by combining the crystal thickness and the beam focusing condition before deciding the best mode. The details of each mode are summarized in Table 1. Single layered crystals are mounted at ST1 port for mode 1. The thickness is doubled for modes 2 and 3 by adding one more layer to each crystal of mode 1. The focusing of diffracted beam is finally applied for mode 3 which becomes the operational arrangement of the facility.

### 3.1. Diffracted Neutron Spectrum

The diffracted neutron spectra were measured by a time-of-flight(TOF) spectrometer[26]. The spectrometer was set up at an adjacent beam port of ST1. The arrangement and setup of the TOF spectrometer are same as those in ref. 11. Total four crystals of 2 mm thickness were used for the measurement. The fractional flux of $n$-th order component in the total diffracted beam was determined from the measured areas of Bragg peaks with correction for the effects of chopper transmission, attenuation and detection efficiency. The peak area was obtained by Gaussian fitting.

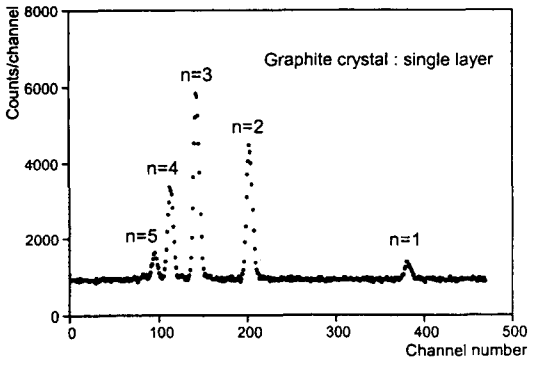


**Fig. 3. Diffracted Neutron TOF Spectrum Measured by a Single Layer of 2 mm Thick Graphite Crystal Set at the Bragg Angle of 45°.**

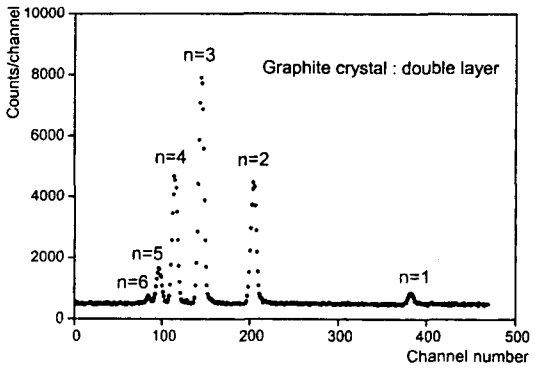


**Fig. 4. Diffracted Neutron TOF Spectrum Measured by Double Layered Crystals Set at the Bragg Angle of 45°.**

**Table 2. Relative Fraction of the Diffracted Neutron Flux from Each Diffraction Order Obtained by a Single Layer of 2 mm Thick Graphite Crystal.**

| Diffraction Order ($n$) | Wavelength [Å] | Energy [meV] | $\phi_D(n)/\phi_D$* [%] | | $\phi_{in}(E)R^E/\phi_{in}$*** |
|---|---|---|---|---|---|
| | | | Calculation | Measurement** | Calculation |
| 1 | 4.74±0.11 | 3.6±0.2 | 6.2 | 6.5±0.4 | 0.0008 |
| 2 | 2.37±0.05 | 14.6±0.7 | 30.2 | 29.5±0.4 | 0.0039 |
| 3 | 1.58±0.04 | 32.8±1.5 | 33.9 | 37.8±0.3 | 0.0043 |
| 4 | 1.19±0.03 | 58.3±2.6 | 19.9 | 19.6±0.2 | 0.0025 |
| 5 | 0.95±0.02 | 91.0±4.1 | 7.7 | 5.4±0.2 | 0.0010 |
| 6 | 0.79±0.02 | 131.1±5.9 | 2.1 | 1.2±0.3 | 0.0003 |

* $\phi_D(n)$ : neutron flux from $n$-th order diffraction, $\phi_D$ : sum of all $\phi_D(n)$' s.

** averaged for two spectra of different crystals.

*** $\phi_{in}$ : total thermal neutron flux of incident beam.

Due to the difficulty of obtaining absolute detection efficiency for the TOF spectrometer, no attempt has been made to get the absolute flux of each Bragg peak. Rather the peaks are compared each other relatively.

One example spectrum for single layered crystal is shown in Fig. 3. Polychromatic components upto the 6$^{th}$ diffraction order are recognized and the pattern of the spectrum is identical with the calculated one in wavelength scale. Bragg peaks of $n$=2,3,4 are dominant. Background in the spectrum arises mostly from the epithermal and fast neutrons which pass the chopper freely. To give the relative fractions for the extraction mode 1, the data for two different crystals are averaged and shown in Table 2. Fig. 4 shows a typical spectrum for double layered crystal. The relative fractions of higher orders increase while those of $n$=1, 2 decrease, seen by comparison with Fig. 3. The peak reflectivity of the first order is more than 0.9 and nearly saturated even for 2 mm thickness. Hence the increase in reflectivity is very small for doubled thickness indicating the severe "secondary extinction" effect. But the reflectivities of higher orders are not saturated at 2 mm thickness and more increase takes place when the crystal

**Table 3. Relative Fraction of the Diffracted Neutron Flux from Each Diffraction Order Obtained by Double Layer of Graphite Crystals.**

| Diffraction Order ($n$) | Wavelength [Å] | Energy [meV] | $\phi_D(n)/\phi_D$* [%] | | $\phi_{in}(E)R^E/\phi_{in}$*** |
|---|---|---|---|---|---|
| | | | Calculation | Measurement** | Calculation |
| 1 | 4.74 ± 0.11 | 3.6 ± 0.2 | 4.5 | 4.4 ± 0.2 | 0.0009 |
| 2 | 2.37 ± 0.05 | 14.6 ± 0.7 | 26.5 | 25.9 ± 0.2 | 0.0054 |
| 3 | 1.58 ± 0.04 | 32.8 ± 1.5 | 35.0 | 39.3 ± 0.3 | 0.0072 |
| 4 | 1.19 ± 0.03 | 58.3 ± 2.6 | 22.4 | 22.9 ± 0.2 | 0.0046 |
| 5 | 0.95 ± 0.02 | 91.0 ± 4.1 | 9.0 | 6.2 ± 0.1 | 0.0019 |
| 6 | 0.79 ± 0.02 | 131.1 ± 5.9 | 2.5 | 1.3 ± 0.1 | 0.0005 |

* averaged for two spectra of different double layer set.

**Table 4. Neutron Flux and Cd-ratio Measured at the Sample Position for Three Extraction Modes of Diffracted Beam.**

| Extraction mode | Neutron flux [n/cm$^2$s] | | Flux gain | | Cd-ratio | |
|---|---|---|---|---|---|---|
| | Calculated | Measured | Calculated | Measured | Calculated | Measured |
| 1 | $2.6\times10^7$ | $2.2\times10^7$ | 1.0 (ref) | 1.0 (ref) | 302 | 292 |
| 2 | $4.1\times10^7$ | $3.5\times10^7$ | 1.6 | 1.6 | 258 | 315 |
| 3 | $7.0\times10^7$ | $6.1\times10^7$ | 1.7 | 1.7 | 258 | 364 |

thickness is doubled. The relative fraction of each diffraction order for the modes 2 and 3 is given in Table 3. The measured fraction is given by averaging the two dataset for double layer. The comparison of measurement and calculation shows that agreement for orders 1, 2, 4 is good while orders 3, 5 have some discrepancy.

### 3.2. Neutron Flux and Cd-ratio

Since it was difficult to measure the diffracted spectrum above the 6$^{th}$ order and to convert the Bragg peak counts into absolute flux, activation method for the bare and Cd-covered gold is used to assess the absolute flux and the epithermal component in the beam. The measurement was carried out for the reactor power of 24 MW in October 2000. Gold wires of 0.1 mm diameter and 0.5 mm thick Cd sheet were used in the measurement. The specific activity of irradiated gold wire was determined by counting the 412 keV $^{198}$Au decay line after irradiation. The counting errors were maintained below 1% level for the bare gold wires and below 3% for Cd-covered wires, respectively. The neutron flux is determined from the specific activity of gold wire and the effective absorption cross section of $^{197}$Au.

Prior to the measurement for the diffracted beam, the white beam flux and its profile incident on the graphite crystals were also determined by similar procedure. In obtaining the absolute white beam flux, the Maxwellian averaged cross section of 85.7 barn was used for $^{197}$Au. The neutron flux at the center of crystal mount is $6.8\times10^9$ n/cm$^2$s with a horizontal variation of 20% and a vertical variation of 8%. The Cd-ratio of white beam is 7.7.

The measurements of the neutron flux and Cd-ratio with the diffracted beam are summarized in Table 4 for the three extraction modes. The effective cross sections used for mode 1 and for

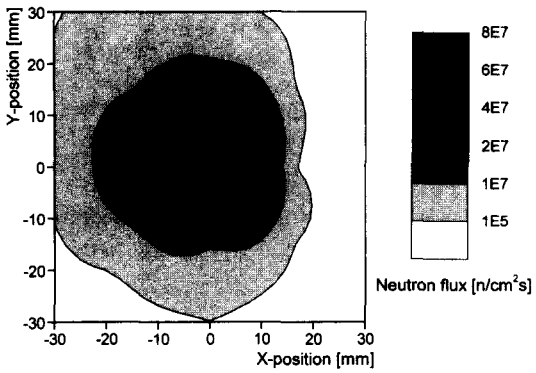


**Fig. 5. Contour Plot of the Beam Profile Measured at the Sample Position.**

modes 2 and 3 are 104.6 and 98.3 barn, respectively. The measured neutron flux and Cd-ratio for the mode 1 are $2.2\times10^7$ n/cm$^2$s and 292, respectively. The flux is increased by a factor of 1.6 in the mode 2 and the focusing gain of 1.7 has been achieved in the mode 3. Both flux gains are in good agreement with the theoretical predictions and the measured flux for each mode is consistent with the theoretical value to within 15%. The Cd-ratio for gold indicates a low but not totally negligible content of epithermal neutron component in the beam. The consistency of Cd-ratio is not comparable to the neutron flux due to the uncertainty of the calculated spectrum in epithermal region. But the calculated values are sufficiently reliable for the order estimation of the Cd-ratio.

The extraction mode was fixed at the mode 3 and the beam size was finally defined upstream of sample by a $^6$LiF slit which has a square opening of $2\times2$ cm$^2$. The flux profile was measured after complete assembling of beam line components. Many gold wire pieces are placed at grid positions on the plane of beam cross section and irradiated. The profiled area is $6\times6$ cm$^2$ and total number of grid points is 65. The grid is spaced in 3 mm step within the central $2\times2$ cm$^2$ area and in 15 mm step outside. Fig. 5 shows a contour plot of the measured beam profile at the sample position. The observed uniformity is less than 12% within the area of $1\times1$ cm$^2$ while abrupt decrease is found outside $2\times2$ cm$^2$. The neutron flux and Cd-ratio are achieved to $7.9\times10^7$ n/cm$^2$s and 266, respectively. The prominent change of flux and Cd-ratio from those in Table 4 is caused by a change in the reactor core between the two measurements, which is the plugging reactor end of ST1 port with Al disk[27]. The modification has resulted in flux enhancement by 30% at the expense of more hardened beam spectrum

**Table 5. Comparison of the Beam Quality with Other PGAA Facilities Using Thermal Neutrons.**

| Facility | Reactor Power | Thermal neutron extraction | Neutron flux [n/cm$^2$s] | Cd-ratio |
|---|---|---|---|---|
| UMd-NIST [1] | 10 MW | Direct beam | $2.0\times10^8$ | 55 |
| Missouri [2] | 10 MW | Filter | $5.0\times10^8$ | 42 |
| Kyoto [28] | 5 MW | Guide tube | $2.0\times10^6$ | n/a* |
| ILL [29] | 57 MW | Guide tube | $1.3\times10^8$ | n/a |
| JAERI [3] | 20 MW | Guide tube | $2.4\times10^7$ | n/a |
| Budapest [4] | 10 MW | Guide tube | $2.0\times10^6$ | n/a |
| Dhruva [7] | 100 MW | Guide tube | $1.4\times10^7$ | 3,040 |
| MIT [15] | 5 MW | Filter & Diffraction | $1.7\times10^7$ | ≥30,000 |
| SNU-KAERI | 24 MW | Diffraction | $7.9\times10^7$ | 266 |

* n/a : not available

certainly. The comparison of the final beam quality with that of some PGAA facilities using thermal neutron is shown in Table 5. The neutron flux of the SNU-KAERI facility is higher than or comparable with those of guided beam while lower than direct beam or Si filtered beam. The pattern of the Cd-ratio is opposite to the neutron flux.

### 3.3. Effective Quantity for Diffracted Beam

Even though the neutron beam spectrum contains all the detailed description of beam characteristics, a simple inclusive way of characterizing beam is suggested for PGAA in terms of the effective velocity and temperature of the beam[30]. These effective values can be deduced from two prescriptive measurements of prompt γ-rays for thin and sufficiently thick samples of any good $1/v$-absorber. Two reference boron samples are provided by NIST, USA[30]. The thin sample is a 2.5 cm square of borophosphosilicate glass with $^{10}B$ areal density of $5\times10^{16}/cm^2$ and the thick sample is a $^{10}B$-Al alloy sheet of 1.3 mm thick, 2.5 cm square with 4.5 wt% $^{10}B$. For the thin sample, the count rate of 478 keV $^{10}B$ peak is given by

$$C_{thin} = \varepsilon\Gamma AD\phi_D\langle\sigma_a\rangle \tag{15}$$

where $\varepsilon$ is the detection efficiency for 478 keV γ-ray, $\Gamma$ is the 478 keV γ-ray yield per neutron capture, $A$ is the sample area and $D$ is the surface density of $^{10}B$. For the thick "black" sample, most of the incident thermal neutrons are captured but a small fraction of the beam can transmit from finite thickness. Hence the count rate is given by

$$C_{thick} = \varepsilon\Gamma A'\phi'_D, \tag{16}$$

where $A' = A\cos45°$ is the projected area of the sample onto the beam cross section since the sample is inclined by 45° with respect to the direction of beam and $\phi'_D$ is the neutron flux which are absorbed by $^{10}B$ in the sample. $\phi'_D$ can be calculated by

$$\phi'_D = \phi_D\sum_n[1-e^{-\Sigma_a(E_n)t}]w_n \tag{17}$$

where $n$ is diffraction order, $\Sigma_a(E_n)$ is macroscopic absorption cross section of $^{10}B$ for neutron of energy $E_n$, the other notations are same as defined before. Although the absorption by $^{11}B$ and $^{27}Al$ enclosed in the sample also exist, the absorption by $^{10}B$ is more than 99.9%. The resultant ratio of $\phi'_D/\phi_D$ is 0.98 due to some transmission for high orders. With this correction into consideration, the measured effective cross section for $^{10}B$ is given by

$$\langle\sigma_a\rangle_{meas} = \frac{A'}{A}\frac{\phi'_D}{\phi_D}\frac{1}{D}\frac{C_{thin}}{C_{thick}} \tag{18}$$

where the last ratio is the measured ratio of count rates.

The γ-ray detector for SNU-KAERI PGAA is an n-type HPGe detector with a relative efficiency of 43%. The signal is processed by a charge sensitive preamplifier, a spectroscopy amplifier and a fast 16k ADC. The ORTEC Gamma-Vision is used for displaying the accumulating spectrum. The normal position of the detector is 25 cm distant from the sample.

The thick sample is irradiated at the normal setup of detection system to find the dead time too severe for quantitative measurement from high count rate. Hence instead of reducing the reference sample size, the actual measurement was performed for the reduced beam flux condition. The white beam collimator was set at 20′. The position of the HPGe detector was changed from 25 cm to the farthest permissible distance, 35 cm and a slab γ-ray collimator with 5 mm wide aperture was added. At the same detection condition, the thin sample was irradiated for longer period. A 6 mm diameter Ti flux monitoring foil was placed at the center of the

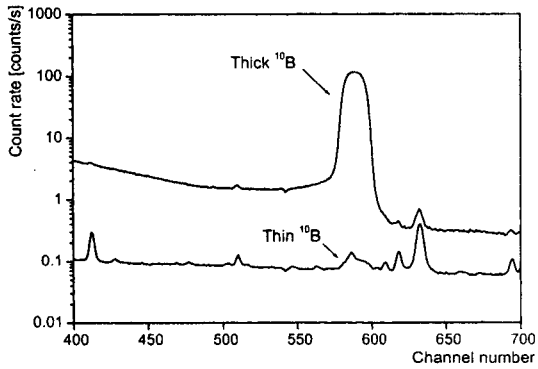


**Fig. 6. Measured Prompt γ-ray Spectra for Thick and Thin Boron Samples.**

sample and co-irradiated. Variation in the average beam flux during the irradiations was less than 1%. An unidentified background peak was found at 475 keV interfering the boron signals and hence the background counts were measured without the sample and subtracted afterwards.

Fig. 6 shows the relevant region of measured spectra for the thick and thin boron samples and Table 6 summarizes the results of counting. The 478 keV $^{10}$B peak is wider than those of typical prompt γ-ray peaks due to Doppler-broadening. In Table 7, the deduced effective values of cross section for $^{10}$B and neutron beam are compared with the values calculated from eqs. (13) and (14). The two results based on boron detection and calculation from spectral information are consistent with each other by 4.5%. The quoted error seems to be underestimated by considering the counting statistics only. The remaining discrepancy can be attributed to the uncertainty of boron surface density $D$ and that of neutron spectrum used in the calculation.

## 4. Conclusions

Beam characteristics of the SNU-KAERI PGAA facility have been investigated by varying the PG crystal thickness and the focusing condition. In assessing the beam spectrum, both the calculated and measured spectra showed the discrete energy pattern of diffracted beam. The 3$^{rd}$ order diffraction is most intense due to closeness of its energy to the peak of incident beam spectrum while the measured TOF spectrum is limited only to the 6$^{th}$ order. Both the calculated and experimental spectra are consistent in the thermal region. The spectrum in the epithermal region is based on the theoretical calculation. Quantitative comparison of the theoretical Cd-ratio with experimental values shows the spectrum in the

**Table 6. Countings of $^{10}$B Peaks for Thin(Borophosphosilicate Glass on Si) and Thick($^{10}$B-Al Alloy) Samples.**

| Sample | Live time [s] | Peak area [counts] | Count rate [cps] |
|---|---|---|---|
| Borophosphosilicate glass on Si | 75000 | 38322±238 | 0.5110± 0.003 |
| $^{10}$B-Al alloy | 3600 | 6.394× $10^6$± 2578 | 1776.1± 0.7 |

**Table 7. Comparison of the Measured Effective Velocity and the Calculated one by Using the Measured Neutron Spectrum and the Energy-dependent Cross Sections of $^{10}$B.**

| | $\langle\sigma_a\rangle$ [barn] | $\langle v\rangle$ [m/s] | $\langle\lambda\rangle$[Å] | $\langle T\rangle$ [K] |
|---|---|---|---|---|
| Measured | 3987.2±39.9 | 2117.2±21.2 | 1.87±0.02 | 268.6±5.4 |
| Calculated | 3806.9 | 2217.4 | 1.78 | 295 |

epithermal region is reasonable even though uncertainty is added for precise characterization. The final neutron flux and Cd-ratio for gold are $7.9 \times 10^7$ n/cm$^2$s and 266, respectively. The effective velocity of $2117 \pm 21$ m/s and the temperature of $269 \pm 5$ K are obtained by measuring the prompt γ-ray spectra for the thin and thick "black" $^{10}$B samples. The full quantitative description of neutron beam and the simple quality of polychromatic diffracted beam with reduced epithermal neutrons and γ-ray backgrounds provide with a unique and competitive facility for PGAA.

## References


1. D.L. Anderson, M.P. Failey, W.H. Zoller, W.B. Walters, G.E. Gordon and R.M. Lindstrom, "Facility for Non-Destructive Analysis for Major and Trace Elements Using Neutron-Capture Gamma-Ray Spectrometry", *J. Radioanal. Chem.* **63**, 97 (1981).
2. A.G. Hanna, R.M. Brugger and M.D. Glascock, "The Prompt Gamma Neutron Activation Analysis Facility at MURR", *Nucl. Instr. and Meth.* **188**, 619 (1981).
3. C. Yonezawa, A.K.H. Wood, M. Hoshi, Y. Ito and E. Tachikawa, "The Characteristics of the Prompt Gamma-Ray Analyzing System at the Neutron Beam Guides of JRR-3M", *Nucl. Instr. and Meth.* A **329**, 207 (1993).
4. Zs. Révay , G.L. Molnár, T. Belgya, Zs. Kasztovszky, R.B. Firestone, "A new gamma-ray spectrum catalog for PGAA," *J. of Radioanal. and Nucl. Chem.* **244**, 383 (2000).
5. R.M. Lindstrom, R. Zeisler, D.H. Vincent, R.R. Greenberg, C.A. Stone, E.A. Mackey, D.L. Anderson and D.D. Clark, "Neutron Capture Prompt Gamma-Ray Activation Analysis at the NIST Cold Neutron Research Facility", *J. Radioanal. Nucl. Chem.* **167**, 121 (1993).
6. M. Crittin, J. Kern, J.-L. Schenker, "The New Prompt Gamma-ray Activation Facility at the Paul Scherrer Institute, Switzerland", *Nucl. Instr. and Meth.* **A 449**, 221 (2000).
7. K. Sudarshan, A.G.C. Nair, R.N. Acharya, Y.M. Scindia, A.V.R. Reddy, S.B. Manohar, A. Goswami, "Capture γ-rays from $^{60}$Co as multi γ-ray efficiency standard for prompt γ-ray neutron activation analysis," *Nucl. Intstr. and Meth.* **A 457**, 180 (2001).
8. D.F.R. Mildner, R. Berliner, O.A. Pringle and J.S. King, " The Small-Angle Neutron Scattering Spectrometer at the University of Missouri Research Reactor", *J. Appl. Cryst.* **14**, 370 (1981).
9. O.K. Harling, J.M. Chabeuf, F. Lambert and G. Yasuda, "A Prompt Gamma Neutron Activation Analysis Facility Using a Diffracted Beam", *Nucl. Instr. and Meth.* **B 83**, 557 (1993).
10. S.H. Byun, H.D. Choi, B.J. Jun and M.S. Kim, "Extraction of Polychromatic Thermal Neutrons by Bragg Diffraction to Use for Prompt Gamma Neutron Activation Analysis", Proceedings of 10$^{th}$ International Symposium on Capture Gamma-Ray Spectroscopy and Related Topics, 731 USA (2000).
11. S.H. Byun and H.D. Choi, "Design Features for a Prompt Gamma Neutron Activation Analysis System at Hanaro", *J. Radioanal. Nucl. Chem.*, **244**, 413 (2000).
12. H.D. Choi, G.M. Sun, S.H. Byun, C.S. Kang and N.B. Kim, "Progress and Plan of the PGNAA Facility at Hanaro", Appendix 3, Summary Report of the Second Research Co-ordination Meeting, INDC(NDS)-**424**, June 2001, IAEA Nuclear Data Section, Vienna, Austria.
13. T.Riste, "Singly Bent Graphite Monochromators for Neutrons", *Nucl. Intstr. and Meth.* **86**, 1 (1970).
14. A.C. Nunes and G. Shirane, "Vertically Bent

Pyrolytic Graphite Crystals Applied to Triple-Axis Neutron Spectrometry", *Nucl. Intstr. and Meth.* **95**, 445 (1971).

15. K.J. Riley and O.K. Harling, "An Improved Prompt Gamma Neutron Activation Analysis Facility Using a Focused Diffracted Neutron Beam", *Nucl. Intstr. and Meth.* **B 143**, 414 (1998).
16. S.H. Byun, H.D. Choi, M.S. Kim and B.J. Jun, "Design of a Prompt Gamma Neutron Activation Analysis System and Neutron Beam Characteristics at Hanaro", Proceedings of the Korea Nuclear Society Spring Meeting, Pohang, Korea, (1999).
17. S.H. Byun, H.D. Choi, M.S. Kim and B.J. Jun, "Measurement of the Moaic Spread of Pyrolytic Graphite Crystals and Focusing Effect of Neutron Beam", Proceedings of the Korea Nuclear Society Autumn Meeting, Seoul, Korea, (1999).
18. S.H. Byun, G.M. Sun, I.J. Kim, H.D. Choi, M.S. Kim and B.J. Jun, "Current Status for Developing the Prompt Gamma Neutron Activation Analysis System at Hanaro", Proceedings of the Korea Nuclear Society Autumn Meeting, Taejeon, Korea, (2000)
19. S.H. Byun, G.M. Sun and H.D. Choi, "Development of a Prompt Gamma Activation Analysis Facility Using Diffracted Polychromatic Neutron Beam", submmited to *Nucl. Intstr. and Meth.* **A**.
20. C.G. Darwin, "The Reflection of X-rays from Imperfect Crystals", *Philos. Mag.* **43**, 800 (1922).
21. G.E. Bacon and R.D. Lowde, "Secondary Extinction and Neutron Crystallography", *Acta. Cryst.* **1**, 303 (1948).
22. V.F. Sears, "Bragg Reflection in Mosaic Crystals. I. General Solution of the Darwin Equations", *Acta. Cryst.* **A 53**, 35 (1997).
23. V.F. Sears, "Neutron Scattering Lengths and Cross Sections", *Neutron News*, **3**, 26 (1992).
24. M. Chabot, P. Nicolai, K. Wohrer, J.P. Rozet, A. Touati, A. Chetioui, D. Vernhet and M.F. Politis, "X-Ray Reflectivities, at Low and High Order of Reflection, of Flat Highly Oriented Pyrolytic Graphite Crystals", *Nucl. Instr. and Meth.* **B 61**, 377 (1991).
25. Evaluated Nuclear Data Files, 1998, http://www.nndc.bnl.gov/nndc/endf/.
26. H.J. Kim, Y.J. Lee, W. Bartl and H.I. Bak, "Time-of-Flight Neutron Spectrometer with a Small Beam Chopper", *Bulletin of the Atomic Energy Research Institute of Korea*, **3**, 9 (1966).
27. B.J. Jun, "Activities for Users in Hanaro", Proceedings of Hanaro Workshop 2000, Taejeon, Korea, 6 (2000).
28. T. Kobayashi and K. Kanda, "Microanalysis System of ppm-Order $^{10}B$ Concentrations in Tissue for Neutron Capture Therapy by Prompt Gamma-Ray Spectrometry", *Nucl. Instr. and Meth.* **204**, 525 (1983).
29. S.A. Kerr, R.A. Oliver, P. Vittoz, G. Vivier, F. Hoyler, T.D. Macmahon and N.I. Ward, "Elemental Concentrations in Geochemical Reference Samples by Neutron Capture Prompt Gamma-Ray Spectroscopy", *J. Radioanal. Nucl. Chem.* **113**, 249 (1987).
30. R.M. Lindstrom, "Neutron Beam Characterization", Appendix 3, Summary Report of the Second Research Co-ordination Meeting, *INDC(NDS)*-**424**, June 2001, IAEA Nuclear Data Section, Vienna, Austria.